Supplementary Information (SI) for Nanoscale Horizons.
This journal is © The Royal Society of Chemistry 2026

Supplementary Information

Stochastic Sampling via Synaptic Delay in Spiking RBMs Using Integrated Resistive and Threshold Switching Devices

Suyeon Jang[†ab], Dae Kyu Lee[†ac], Uicheol Shin[a], Yu Gyeong Kang[ab], Youngsoo Choi[ab], Dongmin Han[ab], Joon Young Kwak[*d] and Sangbum Kim[*ab]

[a] *Department of Materials Science and Engineering, Seoul National University, Seoul 08826, Republic of Korea*
[b] *Inter-University Semiconductor Research Center and Research Institute of Advanced Materials, Seoul 08826, Republic of Korea*
[c] *Center for Semiconductor Technology, Korea Institute of Science and Technology (KIST), Seoul 02792, Republic of Korea*
[d] *Division of Electronic and Semiconductor Engineering, Ewha Womans University, Seoul 03760, Republic of Korea*

† These authors contributed equally to this work.

*Corresponding authors: E-mail addresses: jykwak@ewha.ac.kr and sangbum.kim@snu.ac.kr

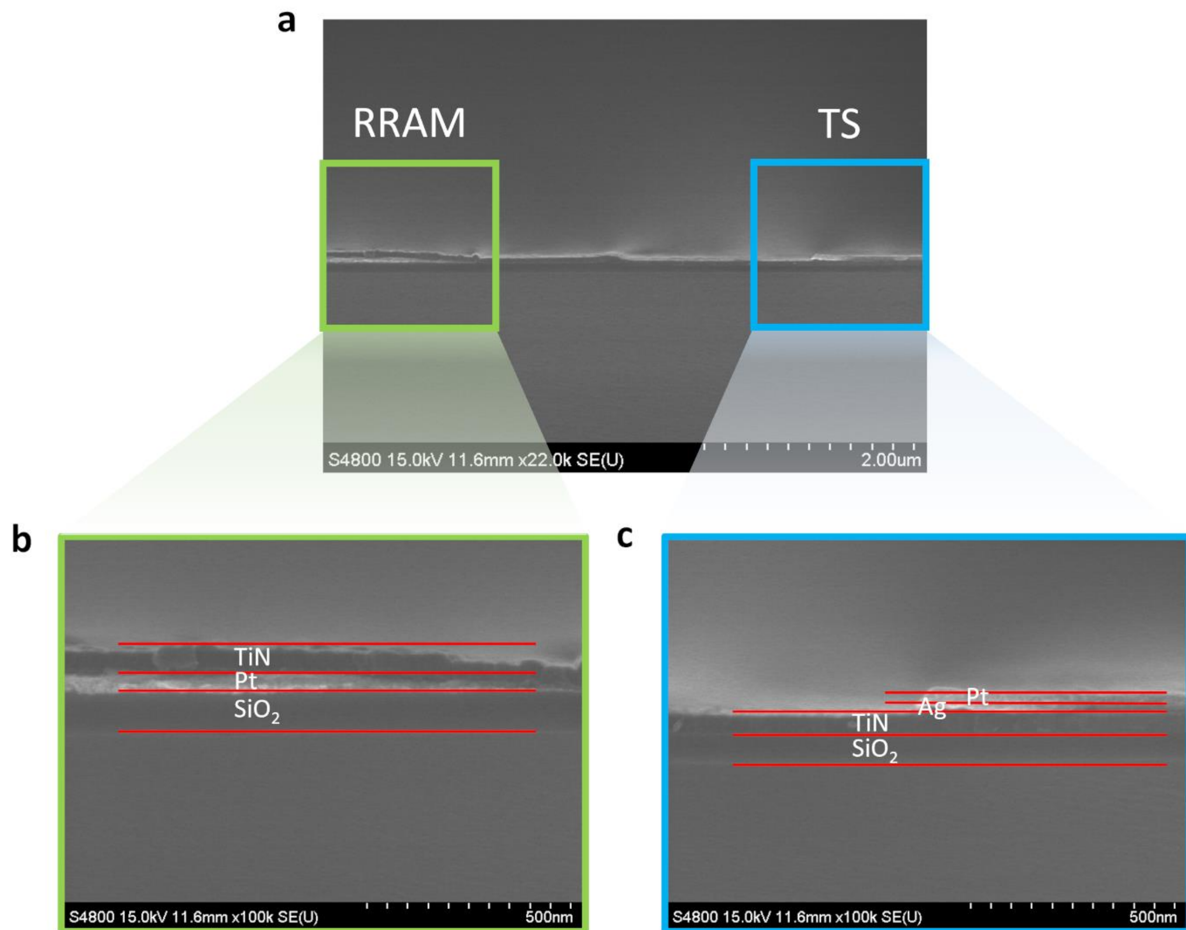

Fig. S1 Cross-sectional scanning electron microscopy (SEM) images of the fabricated RRAM−TS integrated device. (a) Low-magnification cross-sectional SEM image of the integrated structure. Two devices were monolithically integrated by sharing the top electrode of the RRAM and the bottom electrode of the TS. (b) Magnified view of the RRAM device, consisting of TiN/Al_2O_3/HfO_2/Pt/SiO_2 layers. (c) Magnified view of the TS device, consisting of Pt/Ag/HZO/TiN/SiO_2 layers. The thin oxide layers are not clearly resolved due to their small thickness and limited contrast, but are confirmed by cross-sectional HRTEM analysis, as shown in Fig. S2.

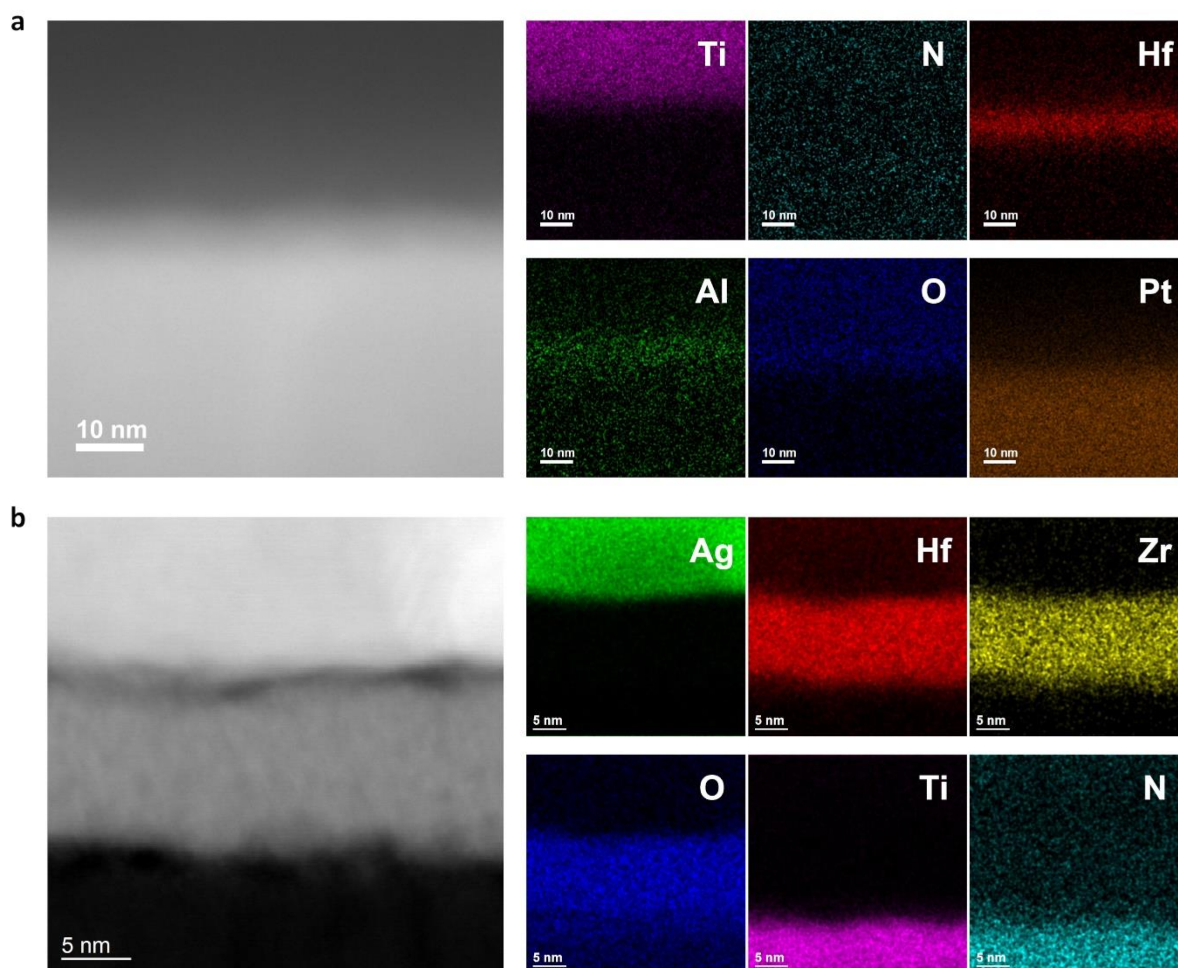

Fig. S2 Cross-sectional transmission electron microscopy (TEM) image and energy dispersive spectroscopy (EDS) analysis of an RRAM−TS device. (a) TEM image and corresponding EDS maps of the RRAM device, showing the distributions of Ti, N, Hf, Al, O, and Pt. (b) TEM image and corresponding EDS maps of the TS device, showing the distributions of Ag, Hf, Zr, O, Ti, and N.

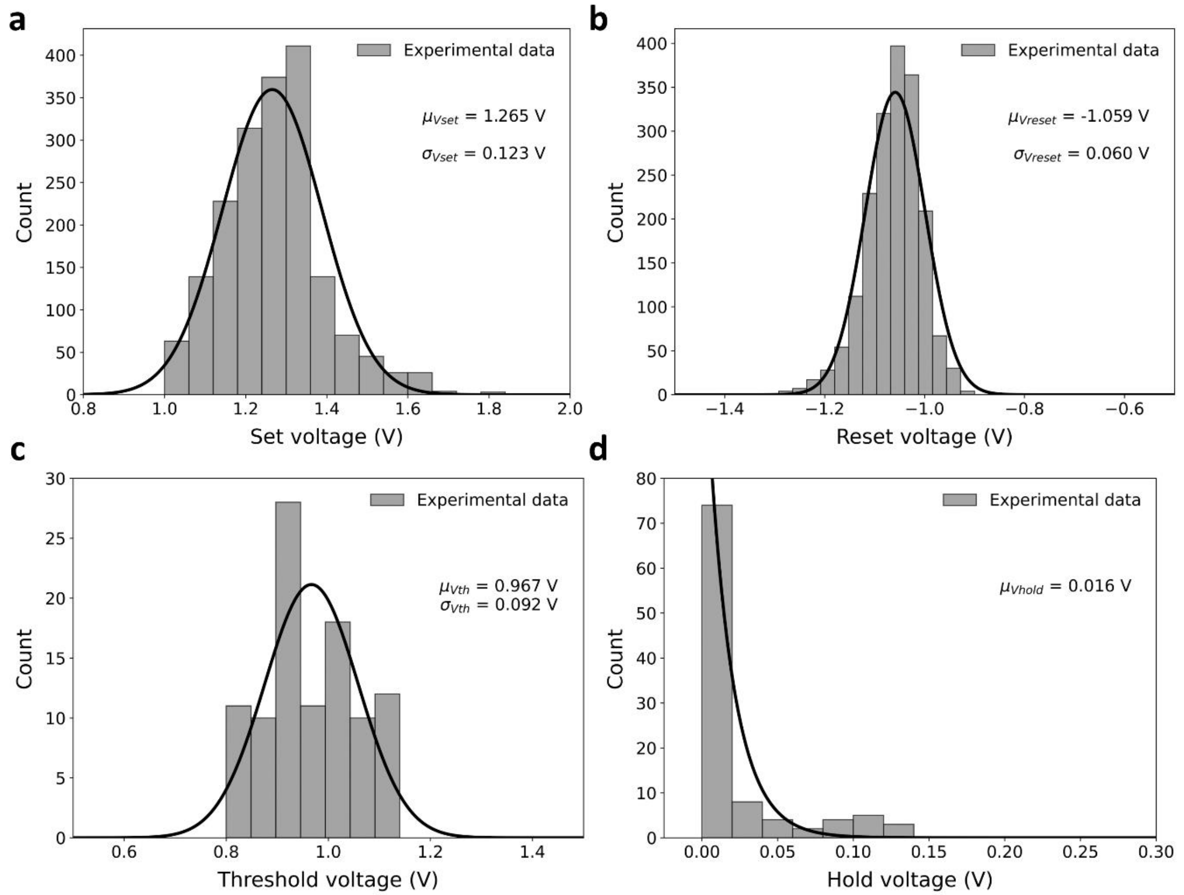

Fig. S3 (a, b) Histograms of the set and reset voltages of the RRAM device measured over 2,000 switching cycles, respectively. The solid curves represent Gaussian fits, yielding μ_{Vset}= 1.265 V, σ_{Vset}= 0.123 V, μ_{Vreset}= −1.059 V, and σ_{Vreset}= 0.060 V. (c, d) Histograms of the threshold and hold voltages of the TS device measured over 100 cycles, respectively. The threshold-voltage distribution was fitted with a Gaussian function, yielding μ_{Vth}= 0.967 V and σ_{Vth}= 0.092 V. Because the hold-voltage distribution is asymmetric and concentrated near 0 V, it was fitted with an exponential function rather than a Gaussian function, yielding μ_{Vhold}= 0.016 V.

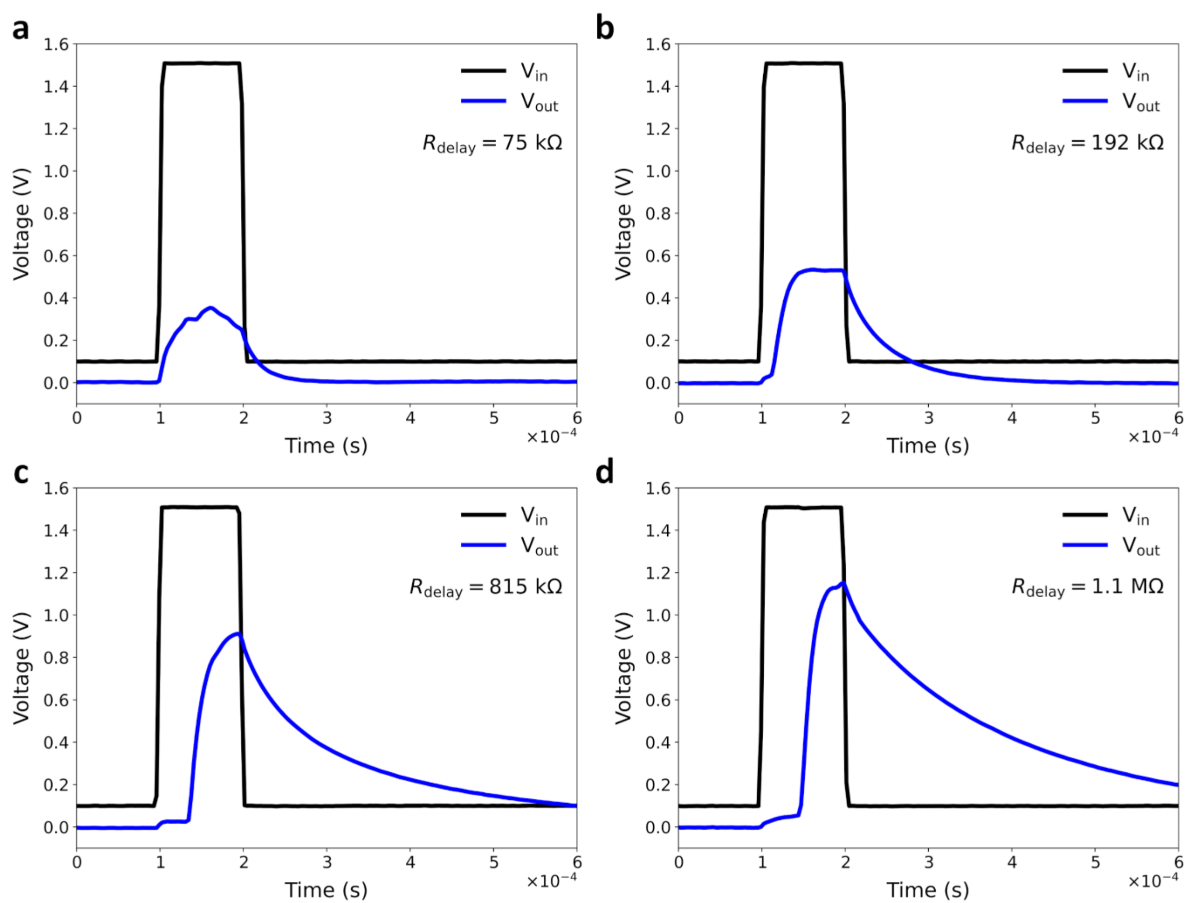

Fig. S4 Pulse responses of the integrated RRAM−TS device measured at different RRAM resistance states. (a–d) Representative voltage transients of the input pulse (V_{in}, black) and output response (V_{out}, blue) measured at R_{delay} = 75 kΩ, 192 kΩ, 815 kΩ, and 1.1 MΩ, respectively.

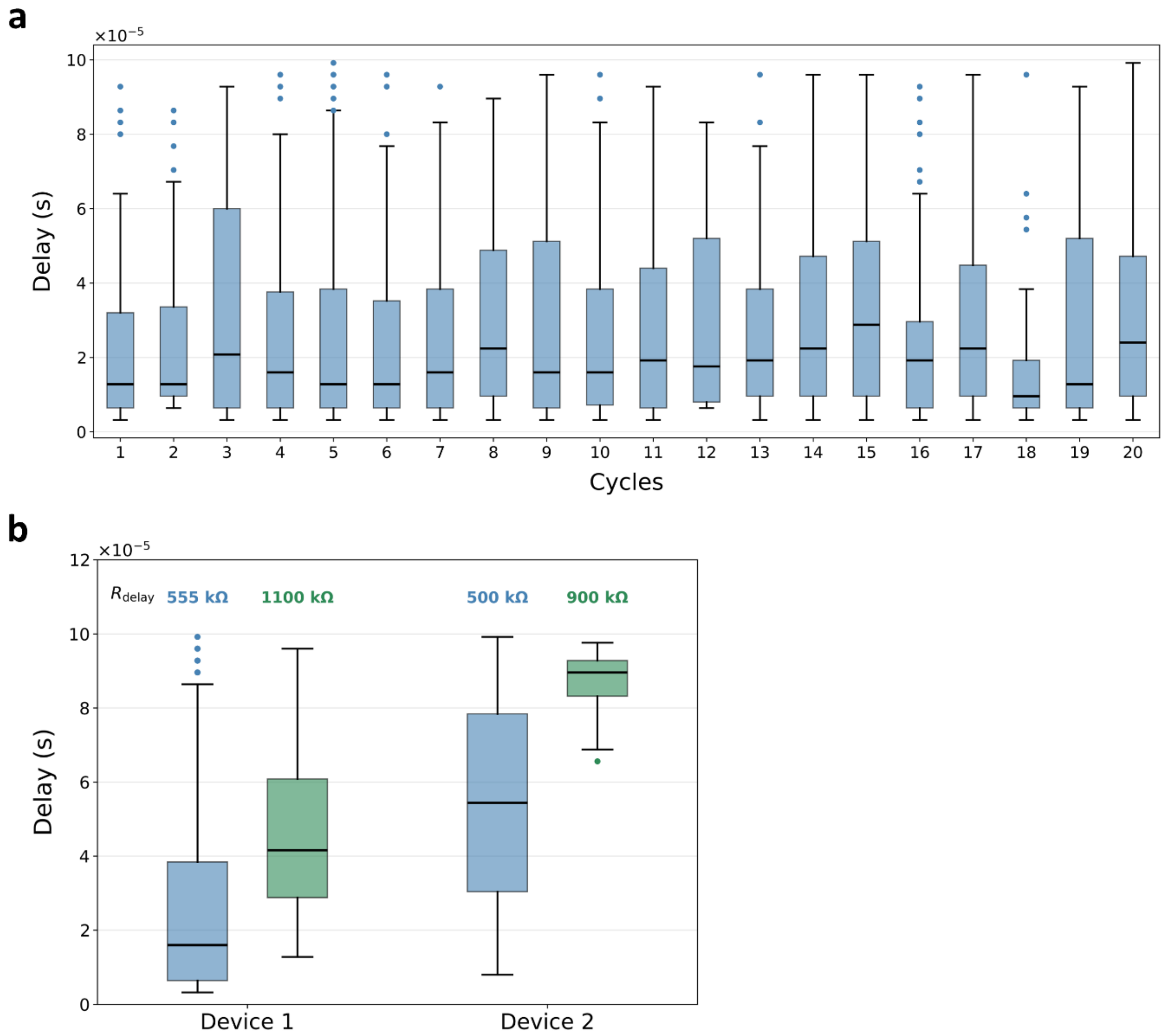

Fig. S5 Stability and reproducibility of the delay distribution in the integrated RRAM−TS delay module. (a) Cycle-to-cycle variation of the delay distribution measured at R_{delay}= 555 kΩ. The delay distribution was obtained by applying 400 input pulses per cycle over 20 repeated cycles. (b) Device-to-device variation of the delay distribution measured from two different integrated RRAM−TS devices. For each device, delay distributions were measured at two R_{delay} states, showing that the delay time increases with increasing R_{delay} despite differences in the absolute delay range between devices.

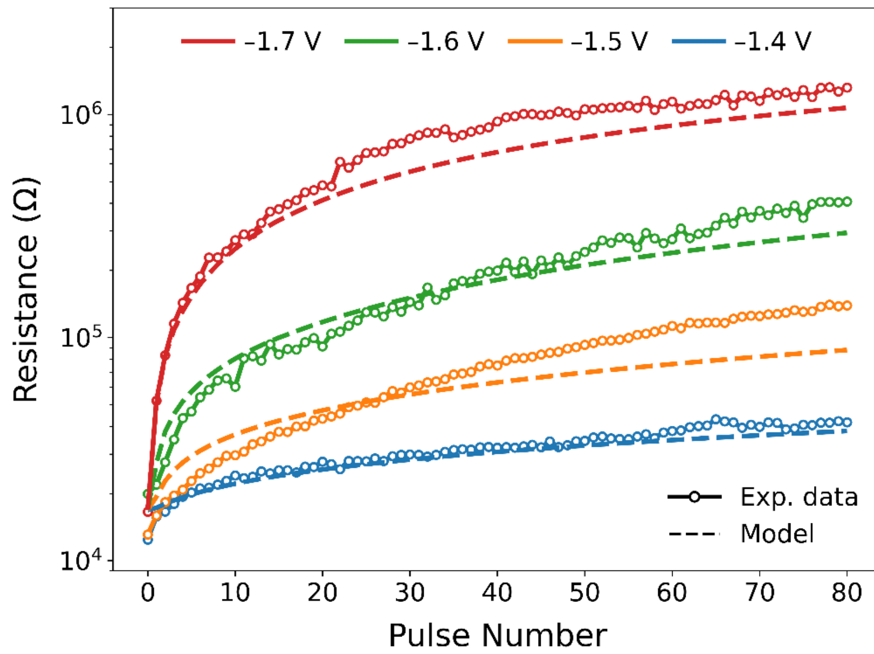

Fig. S6 Experimental and modeled resistance evolution of the RRAM under reset pulse trains. Open circles represent the experimentally measured resistance change induced by identical reset pulse trains with amplitudes of −1.4, −1.5, −1.6, and −1.7 V, and dashed lines represent the corresponding Verilog-A model results. The model reproduces the gradual resistance increase and its dependence on pulse amplitude, supporting its validity for SPICE simulation of the integrated RRAM−TS-based synaptic delay circuit.

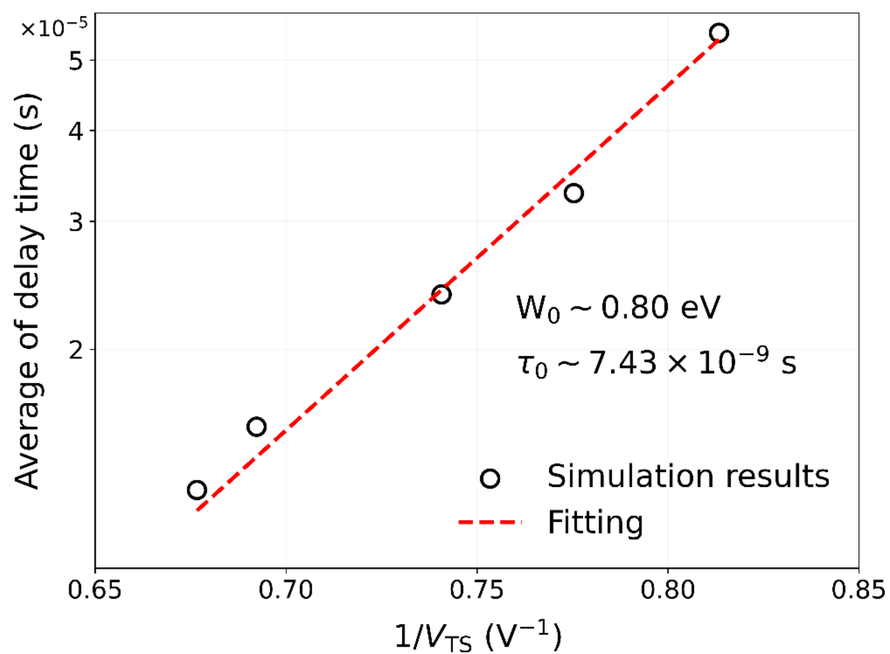

Fig. S7 Relationship between the effective voltage across the TS device and the average delay time obtained from SPICE simulation. Open circles represent the simulated average delay times, and the dashed red line represents the fitting based on the field-induced nucleation model. The fitting yields a nucleation barrier W_0 of approximately 0.80 eV.

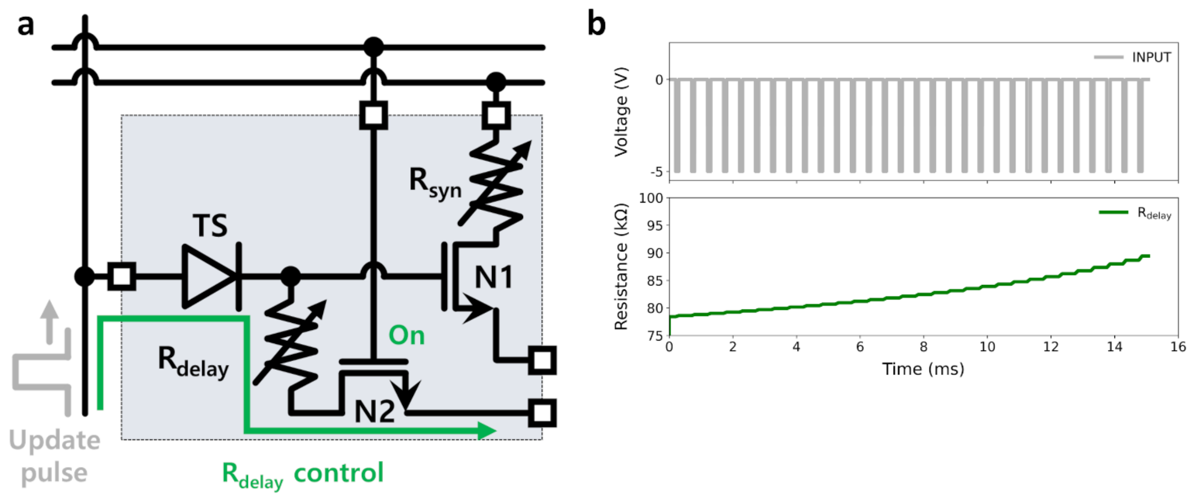

Fig. S8 Programming scheme of R_{delay} in the proposed RRAM−TS-based synaptic delay circuit. (a) Circuit schematic showing the programming path of R_{delay}, where N2 is used to apply update pulses to R_{delay}. (b) Example transient simulation showing the applied update pulse train (top) and the resulting change in R_{delay} over time (bottom).

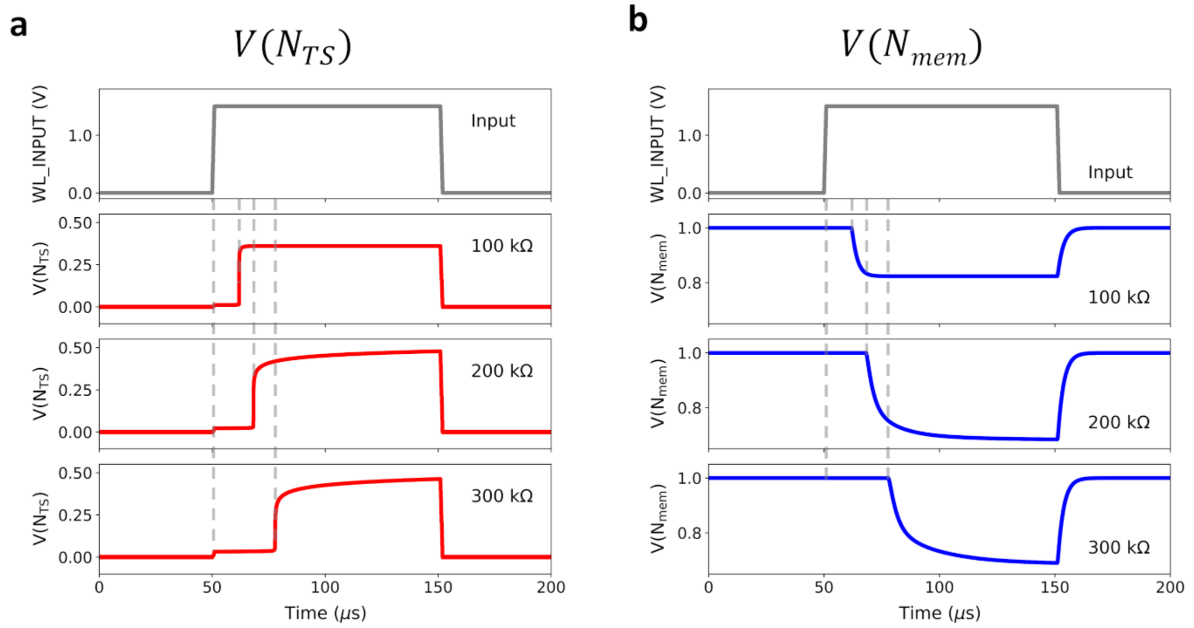

Fig. S9 Simulated temporal responses of the internal TS node and membrane node as a function of R_{delay}. (a) Transient waveforms of the input signal and the delayed pulse generated at the internal node $V(N_{TS})$ for different R_{delay}. (b) Corresponding transient responses of the membrane node voltage $V(N_{mem})$ under the same conditions. The delayed activation induced by increasing R_{delay} modifies the membrane charging dynamics and shifts the temporal response of the neuron circuit.

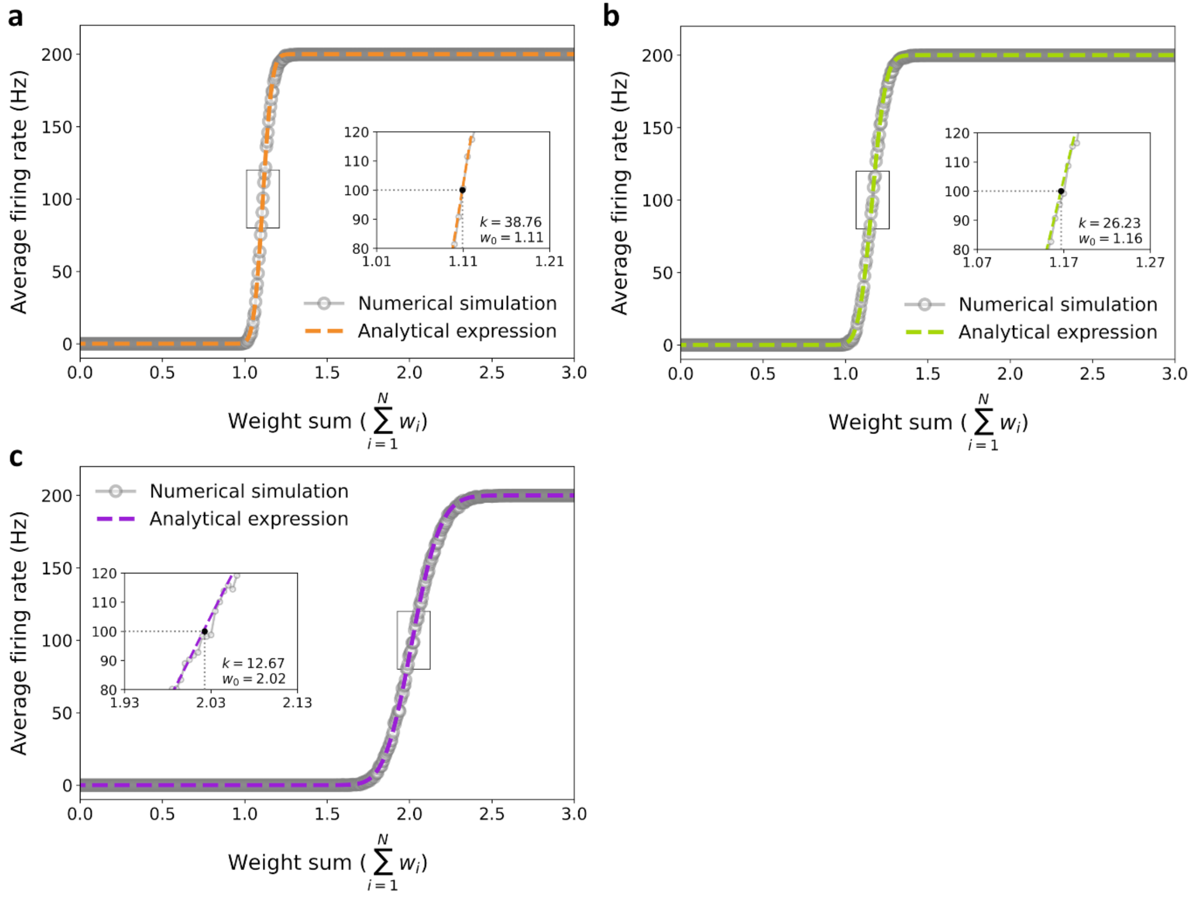

Fig. S10 (a–c) Average firing rate as a function of the total synaptic weight, $\sum_{i=1}^{N} w_i$, for R_{delay}= 75 kΩ, 192 kΩ, and 1.1 MΩ, respectively. Symbols represent the numerical simulation results, and dashed lines represent the analytical expression based on Eq. (8). The insets provide enlarged views of the transition region with sigmoid fits, $y = \frac{200}{1+e^{-k(w-w_0)}}$, highlighting the extracted k and w_0 values.

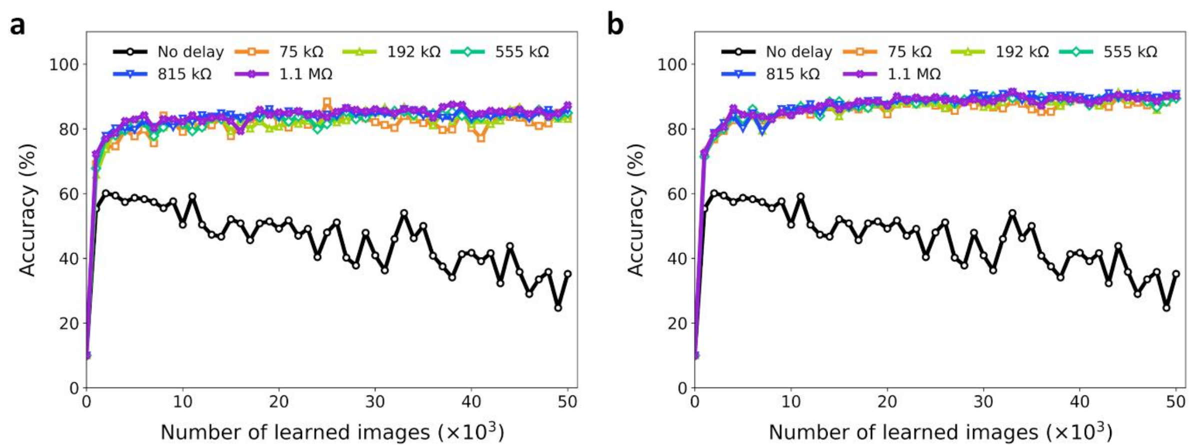

Fig. S11 Learning curves of the spiking RBMs under different R_{delay} conditions for (a) neuronal-delay and (b) synaptic-delay. Compared with the no-delay case, the delay-based models exhibit stable learning behavior, with synaptic-delay providing consistently improved performance over neuronal-delay.

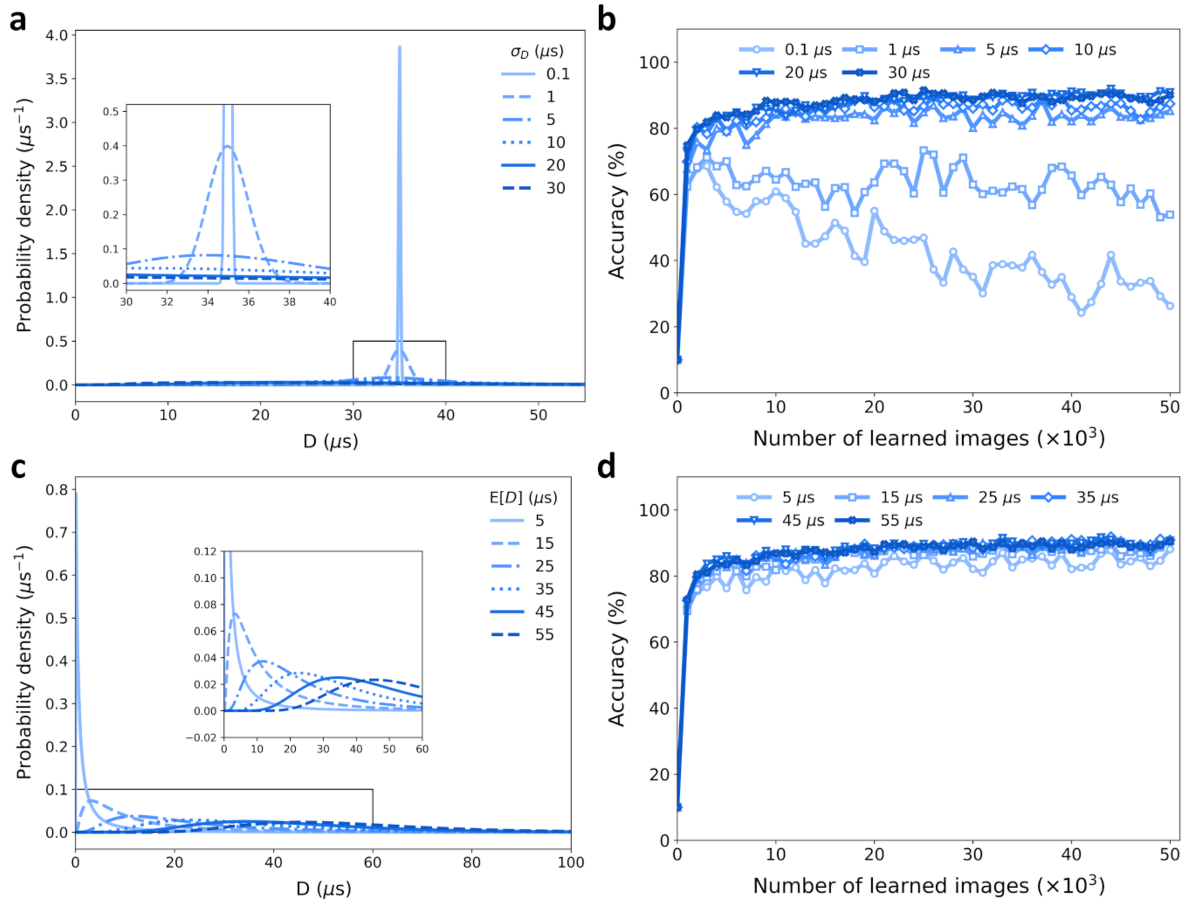

Fig. S12 Delay probability density functions and learning curves corresponding to Figs. 6e and 6f. (a, b) Cases with varying σ_D at a fixed E[D] (=35 μs). (c, d) Cases with varying E[D] at a fixed σ_D (=20 μs). The insets in (a) and (c) provide enlarged views of the highlighted regions. The results confirm that delay variation plays a more critical role than the average delay value in enabling stable learning in spiking RBMs.

a. Cropped image

b. No delay

c. Neuronal delay

d. Synaptic delay

Fig. S13 (a) Cropped input images with one-quarter of the image removed. (b–d) Reconstruction results obtained without delay, with neuronal-delay, and with synaptic-delay, respectively. The delayed cases were generated using the delay distribution corresponding to R_{delay}= 815 kΩ.

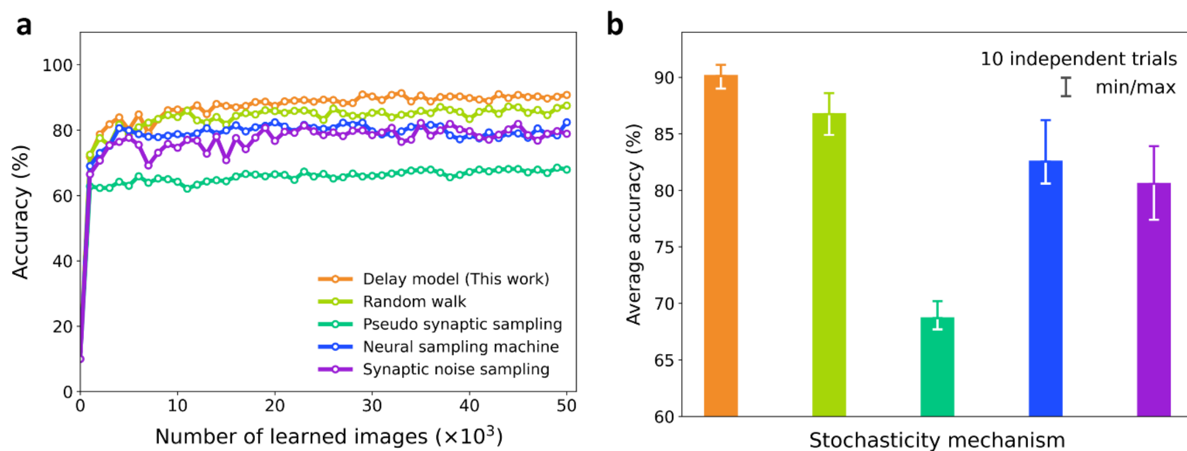

Fig. S14 Comparison of stochastic sampling mechanisms in spiking RBMs. (a) Representative learning curves for different stochasticity mechanisms: the proposed delay model, random walk, pseudo synaptic sampling, neural sampling machine, and synaptic noise sampling. (b) Average accuracy for each stochasticity mechanism over 10 independent trials. The error bars indicate the minimum and maximum values obtained from the 10 independent trials.

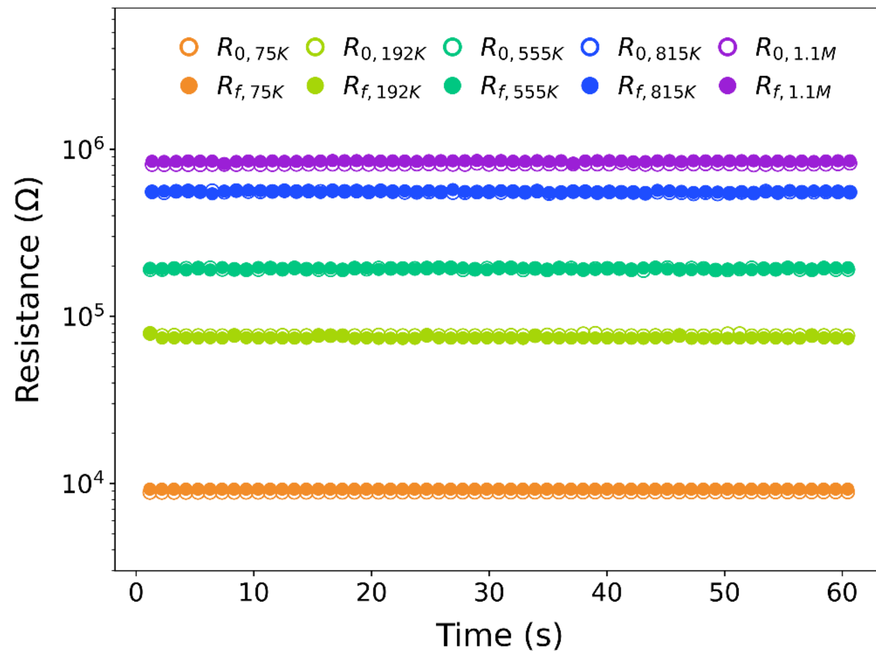

Fig. S15 Retention characteristics of the programmed R_{delay} states under repeated pulse-operation conditions. Open and filled circles represent the initial resistance (R_0) and final resistance (R_f) values, respectively. All programmed states remain stable over time with negligible resistance variation, confirming that the resistance state of the integrated RRAM device is well maintained during delay measurements.

Algorithm 1. Spike propagation of the delay model (i-th neuron → j-th neuron)

Input: Spike spk_i, delay distribution D_{dist} ▷ spk_i: MNIST data
▷ D_{dist}: $LogNormal(\mu, \sigma^2)$

Output: Firing spike new_spk_j

Initialize:

$V_{mem,j} \leftarrow 0$ ▷ Membrane voltage
$V_{init,j} \leftarrow 0$ ▷ Initial voltage
$V_{th,j} \leftarrow 1$ ▷ Threshold voltage
$W_{ij}^{gp} - W_{ij}^{gm} \leftarrow N\ (5.0, 1.06^2)$ ▷ Weight value of synapse
$W_{max} \leftarrow 10$ ▷ Maximum value of weight
$W_{min} \leftarrow 0$ ▷ Minimum value of weight
$\alpha \leftarrow 0.1$ ▷ Normalizing factor for voltage
$T_P \leftarrow 100\ \mu s$ ▷ Maximum pulse width
$new_spk_j \leftarrow$ false ▷ State of new_spk_j

1: **procedure** SPIKE PROPAGATION
2: **while** spk_i is true **do**
3: **if** delay type = neuronal **then**
4: $D \leftarrow D_i \sim D_{dist}$
5: **else if** delay type = synaptic **then**
6: $D \leftarrow D_{ij} \sim D_{dist}$
7: **end if**
8: $a(D) \leftarrow max(0, 1 - D/T_p)$
9: $V_{mem,j} \leftarrow V_{mem,j} + (W_{ij}^{gp} - W_{ij}^{gm}) \times a(D) \times \alpha$
10: **if** $V_{mem,j} \geq V_{th,j}$ **then**
11: $new_spk_j \leftarrow$ true
12: $V_{mem,j} \leftarrow V_{init,j}$
13: **return** new_spk_j ▷ Return $new_spk's\ time$
14: **end if**
15: **end while**
16: **end procedure**

Fig. S16 Pseudo-code of spike propagation with a delay model in spiking RBM simulations. When a spike generated by the i-th neuron is delivered to the j-th neuron in the opposite layer, the delay time D introduced by the delay module reduces the effective conduction time of the input pulse. For neuronal-delay, a single delay value D_i is sampled for each spike event generated by the i-th neuron and is commonly applied to all synapses connected to that neuron. By contrast, for synaptic-delay, an independent delay value D_{ij} is sampled for each synaptic connection (i, j). The resulting effective synaptic weight is then given by $(W_{ij}^{gp} - W_{ij}^{gm}) \times a(D)$, where $a(D) = \max(0, 1 - \frac{D}{T_P})$. This value updates the membrane potential of the j-th neuron, and a new spike is generated when the updated membrane potential exceeds the threshold voltage.

a

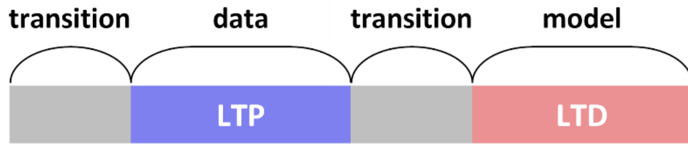

b

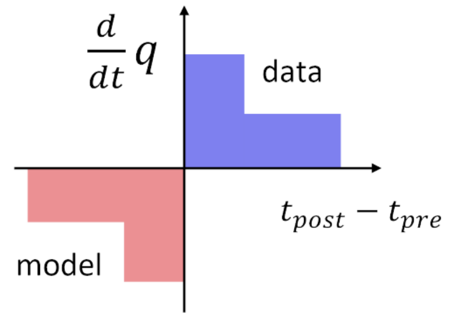

c

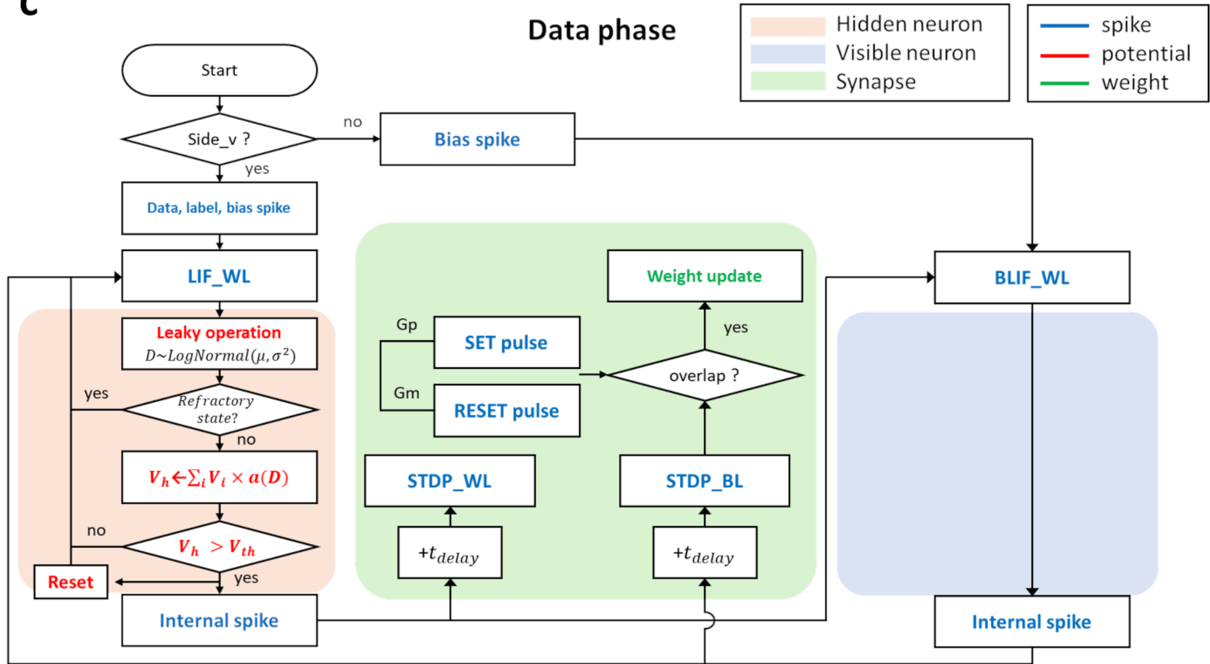

d

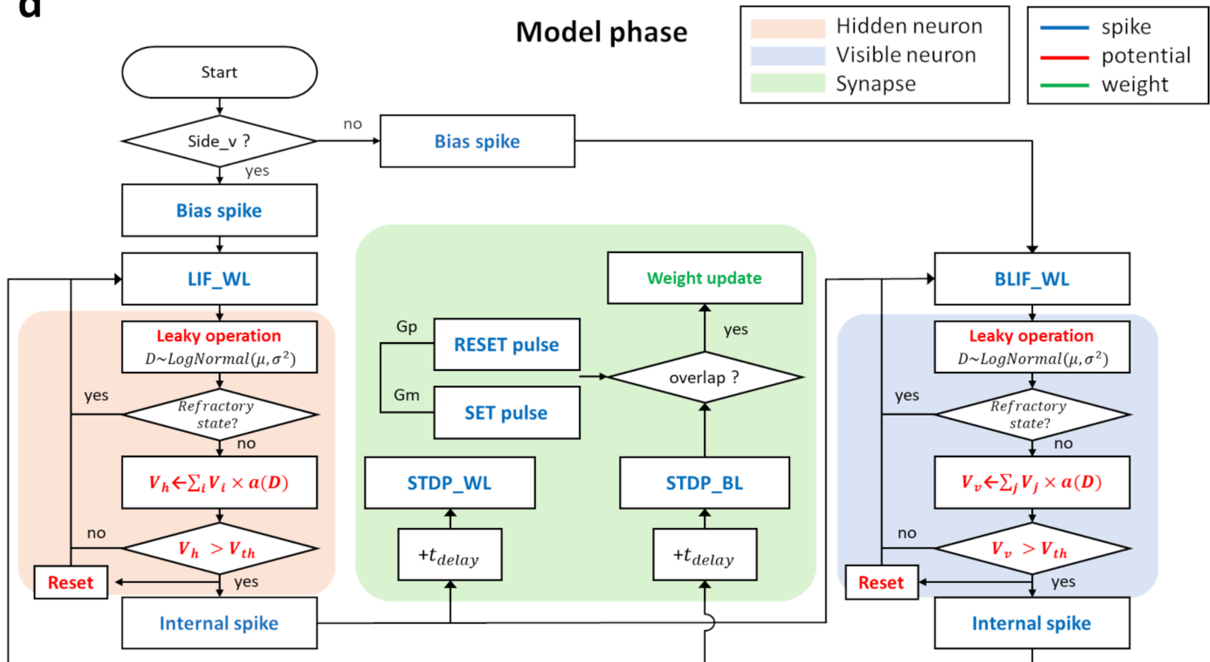

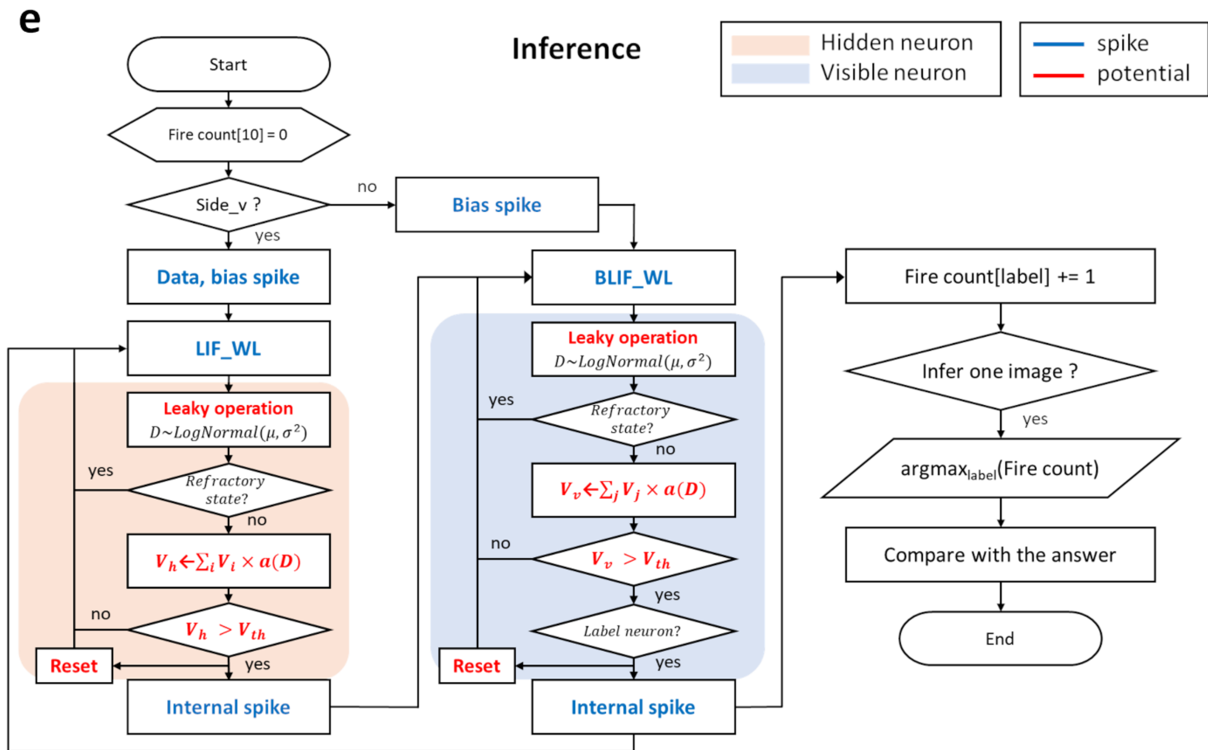

Fig. S17 Schematic diagram illustrating the operation of spiking RBM simulations. (a) Each image is processed through a sequence of transition, data, transition, and model phases. The synaptic weights are potentiated during the data phase and depressed during the model phase. (b) An exponential-like STDP scheme is used, in which a smaller spike-time difference between the pre- and postsynaptic neurons results in a larger weight update. (c–e) Flowcharts of the spiking RBM simulations in the (c) data phase, (d) model phase, and (e) inference stage, respectively, including spike generation, leaky integrate-and-fire neuron dynamics, delay-based spike propagation, and overlap-based weight update.

$lnD \sim N(\mu, \sigma^2)$	RRAM Resistance (Ω)				
	75k	192k	555k	815k	1.1M
μ	-11.6498	-11.5812	-10.9284	-10.4016	-9.9561
σ	1.0477	1.1197	0.9604	0.6398	0.3935
E[D] (μs)	15.10	17.48	28.45	37.29	51.26
σ_D **(μs)**	21.34	27.66	35.03	26.52	20.98

Table S1 Summary of the log-normal fitting parameters for the delay-time distributions measured at different RRAM resistance states within a finite input-pulse window of 100 μs.

Parameters used for the field-induced nucleation model		
α	geometric factor	0.5
E_0	Voltage acceleration factor (MV/cm)	1
d	Device thickness (nm)	10
k	Boltzmann constant (eV/K)	8.62×10^{-5}
T	Ambient temperature (K)	300

Table S2 Fitting parameters used for the field-induced nucleation analysis of the TS delay characteristics.

Parameters used for compact model of TS device				
Material property	a_0	Atomic distance (m) [1]	Fig.3b, 3c, 3d	$0.29 \cdot 10^{-9}$
	σ_{Ag}	Conductivity of Ag (S/m)	Fig.3b, 3c, 3d	10^5
	γ_s	Surface energy (J/m²) [2]	Fig.3b, 3c, 3d	1.0
	Ω	Atomic volume (m³) [1]	Fig.3b, 3c, 3d	$1.7 \cdot 10^{-29}$
	L	Device thickness (m)	Fig.3b, 3c, 3d	10^{-9}
I-V nonlinearity	I_0	Current scaling factor (A)	Fig.3b	$5 \cdot 10^{-14}$
			Fig.3c, 3d	$1 \cdot 10^{-8}$
	V_0	Voltage scaling factor (V)	Fig.3b, 3c, 3d	0.5
	r_{crit}	Critical radius (m)	Fig.3b, 3c, 3d	$0.36 \cdot 10^{-9}$
	r_w	Transition factor of radius (m)	Fig.3b	$0.02 \cdot 10^{-9}$
			Fig.3c, 3d	$0.10 \cdot 10^{-9}$
Thermal model	T_0	Ambient temperature (K)	Fig.3b, 3c, 3d	300
	τ_{th}	Thermal time constant (s)	Fig.3b, 3c, 3d	10^{-10}
	C_{th}	Thermal capacitance (J/K)	Fig.3b, 3c, 3d	$5 \cdot 10^{-17}$
Radius dynamics	γ	Local filed enhancement factor	Fig.3b, 3c, 3d	35
	I_{ref}	Normalization current (A)	Fig.3b	10^{-7}
			Fig.3c, 3d	$7.3 \cdot 10^{-5}$
	r_{min}	Minimum of radius (m)	Fig.3b, 3c, 3d	$0.15 \cdot 10^{-9}$
	r_{max}	Maximum of radius (m)	Fig.3b, 3c, 3d	$0.39 \cdot 10^{-9}$
	v_{set}	Growth velocity prefactor (m/s)	Fig.3b	0.5
			Fig.3c, 3d	0.005
	v_{reset}	Dissolution velocity prefactor (m/s)	Fig.3b, 3c, 3d	0.05
	E_{ag}	Activation energy for growth (eV)	Fig.3b	0.10
			Fig.3c, 3d	0.90
	E_{ar}	Activation energy for dissolution (eV)	Fig.3b, 3c, 3d	0.18

Table S3 List of the parameters used in the TS compact model.[1,2]

Parameters used for the numerical simulation		
$\boldsymbol{N_{pre}}$	Number of presynaptic neuron	100
$\boldsymbol{N_{post}}$	Number of postsynaptic neuron	1
$\boldsymbol{W}$	Weight (w_0 sweep)	$N(w_0, 0.03^2)$
$\boldsymbol{V_{th}}$	Threshold voltage (V)	1.0
$\boldsymbol{V_{reset}}$	Reset voltage (V)	0.0
$\boldsymbol{V_{rest}}$	Resting voltage (V)	0.0
$\boldsymbol{T}$	Input spike period (ms)	5.0
$\boldsymbol{\tau_{mem}}$	Membrane time constant (ms)	1.0
$\boldsymbol{\tau_{ref}}$	Refractory time (ms)	4.0

Table S4 List of the parameters used in the numerical simulations. The simulations were conducted by sweeping w_0.

Parameters used for the spiking RBM simulations			
N_v (N_{data}, N_{label}, N_{bias})	Number of visible neurons	All methods	832 (784, 40, 8)
N_h (N_{hidden}, N_{bias})	Number of hidden neurons		832 (824, 8)
$N_{Training}$	Number of training images per iteration		100 / label
$N_{Inference}$	Number of inference images per iteration		100 / label
$N_{iteration}$	Number of training iteration		50
W_0	Initial weight		$N(0.0, 0.15^2)$
η	learning rate		0.001
T_{image}	Total time for one training image (ms)		0.1
R_{input}	Input spike rate (Hz)		200
V_{th}	Threshold voltage (V)		1.0
V_{reset}	Reset voltage (V)		0.0
V_{rest}	Resting voltage (V)		0.0
τ_{mem}	Membrane time constant (ms)		1.0
τ_{ref}	Refractory time (ms)		4.0
V_{RW}	Voltage steps	Random walk	0.05
$p_{sampling}$	Sampling probability	Random walk Pseudo synaptic sampling Neural sampling machine	0.5
D_{noise}	Multiplicative noise distribution	Synaptic noise sampling	$N(1.0, 0.015^2)$

Table S5 List of the parameters used in the spiking RBM simulations. The common parameters were applied to all stochastic sampling methods, whereas the method-specific parameters were varied according to each sampling scheme.

Note S1 Derivation of the firing rate expression under log-normally distributed delay

To account for temporal variability in spike transmission, the delay D is assumed to follow a log-normal distribution,

$$\ln D \sim N(\mu, \sigma^2),$$

with probability density function

$$f_D(d) = \frac{1}{d\sigma\sqrt{2\pi}} \exp\left[-\frac{(\ln d - \mu)^2}{2\sigma^2}\right], \quad d > 0.$$

When a presynaptic spike is delayed by D, the effective integration window is reduced. The corresponding effective time factor is defined as

$$a(D) = \max\left(0, 1 - \frac{D}{T_P}\right),$$

where T_P denotes the pulse width. Since $a(D) = 0$ for $D \geq T_P$, its moments can be evaluated over the interval $0 \leq d \leq T_P$.

To derive the moments of $a(D)$, consider first the truncated moment of a log-normal random variable:

$$\int_0^{T_P} d^k f_D(d) dd.$$

Using the substitution $y = \ln d$, this becomes

$$\int_0^{T_P} d^k f_D(d) dd = \int_{-\infty}^{\ln T_P} \frac{1}{\sigma\sqrt{2\pi}} \exp\left(ky - \frac{(y-\mu)^2}{2\sigma^2}\right) dy.$$

Completing the square yields

$$ky - \frac{(y-\mu)^2}{2\sigma^2} = -\frac{(y - (\mu + k\sigma^2))^2}{2\sigma^2} + k\mu + \frac{k^2\sigma^2}{2},$$

and therefore

$$\int_0^{T_P} d^k f_D(d) dd = \exp\left(k\mu + \frac{k^2\sigma^2}{2}\right) \Phi\left(\frac{\ln T_P - (\mu + k\sigma^2)}{\sigma}\right),$$

where $\Phi(\cdot)$ denotes the cumulative distribution function of the standard normal distribution.

Using these results, the first moment of $a(D)$ is

$$E[a(D)] = \int_0^{T_P} \left(1 - \frac{d}{T_P}\right) f_D(d) dd$$
$$= \Phi\left(\frac{\ln T_P - \mu}{\sigma}\right) - \frac{1}{T_P} \exp\left(\mu + \frac{\sigma^2}{2}\right) \Phi\left(\frac{\ln T_P - (\mu + \sigma^2)}{\sigma}\right).$$

Similarly, the second moment is

$$E[a(D)^2] = \int_0^{T_P} \left(1 - \frac{d}{T_P}\right)^2 f_D(d) dd$$
$$= \Phi\left(\frac{\ln T_P - \mu}{\sigma}\right) - \frac{2}{T_P} \exp\left(\mu + \frac{\sigma^2}{2}\right) \Phi\left(\frac{\ln T_P - (\mu + \sigma^2)}{\sigma}\right) + \frac{1}{T_P^2} \exp(2\mu + 2\sigma^2)\, \Phi\left(\frac{\ln T_P - (\mu + 2\sigma^2)}{\sigma}\right).$$

Thus, the variance of the effective time factor is given by

$$Var[a(D)] = E[a(D)^2] - E[a(D)]^2.$$

Next, consider a postsynaptic neuron receiving regular presynaptic spikes with period T. Let u_t^- denote the membrane voltage immediately before the input arriving at time step t, and let Δu_t denote the instantaneous membrane voltage increment induced by that input. Then the voltage immediately after the input is

$$u_t^+ = u_t^- + \Delta u_t.$$

Between consecutive inputs, the membrane voltage decays exponentially with membrane time constant τ_m. Therefore,

$$u_{t+1}^- = u_t^+ e^{-\frac{T}{\tau_m}}.$$

Defining

$$\alpha = e^{-\frac{T}{\tau_m}},$$

the update equation becomes

$$u_{t+1}^- = \alpha(u_t^- + \Delta u_t).$$

Assuming that Δu_t is independent and identically distributed (i.i.d.) across time, the steady-state mean of u^- satisfies

$$E[u^-] = \alpha(E[u^-] + E[\Delta u]),$$

which gives

$$E[u^-] = \frac{\alpha E[\Delta u]}{1-\alpha}.$$

The steady-state mean immediately after input arrival is

$$E[u^+] = E[u^-] + E[\Delta u] = \frac{E[\Delta u]}{1-\alpha}.$$

The steady-state variance of u^- is obtained from

$$Var[u^-] = \alpha^2 Var[u^- + \Delta u].$$

Under the i.i.d. assumption, u^- and Δu are independent, so that

$$Var[u^-] = \frac{\alpha^2 Var[\Delta u]}{1-\alpha^2}.$$

Therefore,

$$Var[u^+] = Var[u^-] + Var[\Delta u] = \frac{Var[\Delta u]}{1-\alpha^2}.$$

If the postsynaptic neuron receives inputs from N presynaptic neurons with synaptic weights w_{ij}, and each input is attenuated by the delay-dependent factor $a(D)$, then the total voltage increment at each input event is

$$\Delta u = \sum_{i=1}^{N} w_{ij}\, a(D_i),$$

where the delays D_i are assumed to be i.i.d. The mean and variance of Δu are then given by

$$E[\Delta u] = \sum_{i=1}^{N} w_{ij}\, E[a(D)], \qquad and \qquad Var[\Delta u] = \sum_{i=1}^{N} w_{ij}^2\, Var[a(D)].$$

Substituting into the steady-state expressions yields

$$E[u^+] = \frac{\sum_{i=1}^{N} w_{ij}\, E[a(D)]}{1-\alpha}, \qquad and \qquad Var[u^+] = \frac{\sum_{i=1}^{N} w_{ij}^2\, Var[a(D)]}{1-\alpha^2}.$$

Finally, the firing rate is determined by the probability that the membrane voltage immediately after an input exceeds the threshold u_{th}. Since inputs arrive periodically with frequency $1/T$,

$$\nu = \frac{1}{T}\Pr(u^+ \geq u_{th}).$$

Approximating u^+ as Gaussian with the above mean and variance gives,

$$\nu = \frac{1}{T}\left[1 - \Phi\left(\frac{u_{th} - E[u^+]}{\sqrt{Var[u^+]}}\right)\right] = \frac{1}{2T}\left[1 + \mathrm{erf}\left(\frac{E[u^+] - u_{th}}{\sqrt{2Var[u^+]}}\right)\right].$$

Substituting the explicit expressions for $E[u^+]$ and $Var[u^+]$, the firing rate can be written as

$$\nu = \frac{1}{2T}\left[1 + \mathrm{erf}\left(\frac{\frac{\sum_{i=1}^{N} w_{ij}\, E[a(D)]}{1-\alpha} - u_{th}}{\sqrt{\frac{2\sum_{i=1}^{N} w_{ij}^2\, Var[a(D)]}{1-\alpha^2}}}\right)\right].$$

This expression explicitly shows how the statistics of the log-normally distributed delay modulate the neuronal firing rate through the mean and variance of the effective time factor $a(D)$.

References

1. K. Hermann, *Crystallography and surface structure: an introduction for surface scientists and nanoscientists*, Wiley-VCH, Weinheim, Germany, 2011.
2. W. Wang, M. Wang, E. Ambrosi, A. Bricalli, M. Laudato, Z. Sun, X. Chen and D. Ielmini, *Nat. Commun.*, 2019, **10**, 81.